

June 2016

Small-angle X-ray Scattering Studies of the Oligomeric State and Quaternary Structure of the Trifunctional Proline Utilization A (PutA) Flavoprotein from *Escherichia coli*

Ranjan K. Singh
University of Missouri-Columbia

John D. Larson
University of Missouri-Columbia

Weidong Zhu
University of Nebraska - Lincoln

Robert P. Rambo
Lawrence Berkeley National Laboratory, Berkeley

Greg L. Hura
Lawrence Berkeley National Laboratory, Berkeley

Follow this and additional works at: <https://digitalcommons.unl.edu/biochemfacpub>

 Part of the [Biochemistry Commons](#), [Biotechnology Commons](#), and the [Other Biochemistry, Biophysics, and Structural Biology Commons](#)

Singh, Ranjan K.; Larson, John D.; Zhu, Weidong; Rambo, Robert P.; Hura, Greg L.; Becker, Donald F.; and Tanner, John J., "Small-angle X-ray Scattering Studies of the Oligomeric State and Quaternary Structure of the Trifunctional Proline Utilization A (PutA) Flavoprotein from *Escherichia coli*" (2016). *Biochemistry -- Faculty Publications*. 181.
<https://digitalcommons.unl.edu/biochemfacpub/181>

This Article is brought to you for free and open access by the Biochemistry, Department of at DigitalCommons@University of Nebraska - Lincoln. It has been accepted for inclusion in Biochemistry -- Faculty Publications by an authorized administrator of DigitalCommons@University of Nebraska - Lincoln.

Authors

Ranjan K. Singh, John D. Larson, Weidong Zhu, Robert P. Rambo, Greg L. Hura, Donald F. Becker, and John J. Tanner

Small-angle X-ray Scattering Studies of the Oligomeric State and Quaternary Structure of the Trifunctional Proline Utilization A (PutA) Flavoprotein from *Escherichia coli*[§]

Received for publication, August 15, 2011, and in revised form, October 17, 2011 Published, JBC Papers in Press, October 19, 2011, DOI 10.1074/jbc.M111.292474

Ranjan K. Singh[‡], John D. Larson[‡], Weidong Zhu[§], Robert P. Rambo[¶], Greg L. Hura[¶], Donald F. Becker[§], and John J. Tanner^{‡¶||1}

From the Departments of [‡]Chemistry and ^{||}Biochemistry, University of Missouri-Columbia, Columbia, Missouri 65211, the [§]Department of Biochemistry, University of Nebraska-Lincoln, Lincoln, Nebraska 68588, and the [¶]Lawrence Berkeley National Laboratory, Berkeley, California 94720

Background: Trifunctional proline utilization A (PutA) proteins are multifunctional flavoproteins that catalyze two reactions and repress transcription of the *put* regulon.

Results: PutA from *Escherichia coli* is a V-shaped dimer, with the DNA-binding domain mediating dimerization.

Conclusion: Oligomeric state and quaternary structures are not conserved by PutAs.

Significance: The first three-dimensional structural information for any trifunctional PutA is reported.

The trifunctional flavoprotein proline utilization A (PutA) links metabolism and gene regulation in Gram-negative bacteria by catalyzing the two-step oxidation of proline to glutamate and repressing transcription of the proline utilization regulon. Small-angle x-ray scattering (SAXS) and domain deletion analysis were used to obtain solution structural information for the 1320-residue PutA from *Escherichia coli*. Shape reconstructions show that PutA is a symmetric V-shaped dimer having dimensions of 205 × 85 × 55 Å. The particle consists of two large lobes connected by a 30-Å diameter cylinder. Domain deletion analysis shows that the N-terminal DNA-binding domain mediates dimerization. Rigid body modeling was performed using the crystal structure of the DNA-binding domain and a hybrid x-ray/homology model of residues 87–1113. The calculations suggest that the DNA-binding domain is located in the connecting cylinder, whereas residues 87–1113, which contain the two catalytic active sites, reside in the large lobes. The SAXS data and amino acid sequence analysis suggest that the Δ^1 -pyrroline-5-carboxylate dehydrogenase domains lack the conventional oligomerization flap, which is unprecedented for the aldehyde dehydrogenase superfamily. The data also provide insight into the function of the 200-residue C-terminal domain. It is proposed that this domain serves as a lid that covers the internal substrate channeling cavity, thus preventing escape of the catalytic intermediate into the bulk medium. Finally, the SAXS model is consistent with a cloaking mechanism of gene regulation whereby interaction of PutA with the membrane hides the DNA-binding surface from the *put* regulon thereby activating transcription.

Proline catabolism in Gram-negative bacteria is catalyzed by the bifunctional enzyme proline utilization A (PutA)² (1, 2). The catalytic apparatus of PutAs consists of an FAD-dependent proline dehydrogenase (PRODH) active site that catalyzes the oxidation of proline to Δ^1 -pyrroline-5-carboxylate (P5C), and an NAD⁺-dependent P5C dehydrogenase (P5CDH) active site that catalyzes the oxidation of glutamate semialdehyde to glutamate (Fig. 1). These two reactions are linked by a hydrolysis step that converts P5C into glutamate semialdehyde.

In addition, some PutAs provide genetic regulation by acting as transcriptional repressors, thereby establishing a class of trifunctional PutAs (3–9). The best studied trifunctional PutA is EcPutA from *Escherichia coli* (5, 10–17). EcPutA controls the expression of the *put* regulon, which contains the genes encoding EcPutA and the proline transporter PutP. When proline levels are low, EcPutA blocks transcription by binding to operator sites located between the two divergently transcribed genes. Increased proline levels cause EcPutA to dissociate from DNA and bind the inner membrane, which activates gene transcription, uptake of proline, and proline catabolic enzymatic activity. The mechanism by which proline stimulates proline utilization, e.g. functional switching, involves global conformational changes induced by proline reduction of the FAD, which enhance membrane binding affinity and shift the equilibrium of PutA from DNA-bound to membrane-associated. Thus, trifunctional PutAs are dynamic proteins that function both as a sensor that monitors the level of environmental proline and a transducer that converts proline into usable energy for the organism.

* This work was supported, in whole or in part, by National Institutes of Health Grants GM065546 and GM061068.

[§] The on-line version of this article (available at <http://www.jbc.org>) contains supplemental Figs. S1–S6.

¹ To whom correspondence should be addressed. Tel.: 573-884-1280; Fax: 573-882-2754; E-mail: tannerjj@missouri.edu.

² The abbreviations used are: PutA, proline utilization A; PRODH, proline dehydrogenase; P5C, Δ^1 -pyrroline-5-carboxylate; P5CDH, Δ^1 -pyrroline-5-carboxylate dehydrogenase; BjPutA, *B. japonicum* proline utilization A; EcPutA, *E. coli* proline utilization A; RHH, ribbon helix helix; CTD, EcPutA C-terminal domain of unknown function; CCM, conserved C-terminal motif; PDB, Protein Data Bank; SAXS, small-angle X-ray scattering; SEC, size exclusion chromatography; MALS, multiangle light scattering; PutA1–1085, domain deletion mutant of EcPutA having residues 1–1085; PutA86–1320, domain deletion mutant of EcPutA having residues 86–1320; TEVP, tobacco etch virus protease.

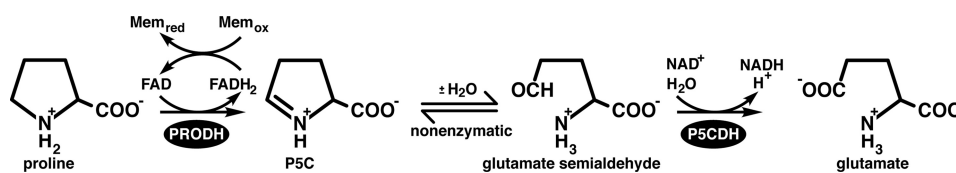


FIGURE 1. Reactions catalyzed by PutA.

The crystal structure of a bifunctional PutA is known (18) (supplemental Fig. S1). At 999 residues, PutA from *Bradyrhizobium japonicum* (BjPutA) is among the smallest of PutAs and is therefore considered to be a minimalist PutA. The PRODH active site is located in a $(\beta\alpha)_8$ barrel, whereas the P5CDH site resides in a crevice between the Rossmann-like NAD^+ -binding domain and the catalytic domain that furnishes the essential reactive Cys. The two active sites are separated by 41 Å and connected by a large, irregularly shaped internal cavity (silver surface in supplemental Fig. S1A). It has been hypothesized that the cavity functions in substrate channeling by serving as an internal reaction vessel for the hydrolysis of P5C to glutamate semialdehyde and a protected conduit for the diffusion of the semialdehyde to the P5CDH active site. In addition to the catalytic domains, the structure includes four ancillary domains (arm, α , linker, and oligomerization) that not only help to create the aforementioned cavity, but also provide the sites for oligomerization. Of particular note for the current work is the oligomerization domain.

The oligomerization domain of BjPutA is a bipartite flap consisting of a β -hairpin and the C-terminal ~ 20 residues of the chain (supplemental Fig. S1A, orange). The latter part of the oligomerization domain forms a β -strand followed by a turn of α -helix and contains the conserved sequence motif EXXXv(N or D)t(T or A)AaGGnaXL, where uppercase, lowercase, and X indicate identical, highly conserved, and any residue, respectively. The sequence appears to be in all branch 1 PutAs, a group that includes both BjPutA and trifunctional PutAs (1). BjPutA forms a domain-swapped dimer in which the flap of one protomer forms main chain hydrogen bonds with the β -sheet of the catalytic domain of the other protomer (supplemental Fig. S1B). As a consequence of dimerization, the flap of one protomer seals the cavity of the other protomer from the bulk medium preventing loss of the intermediate (supplemental Fig. S1C).

Trifunctional PutAs have two additional domains not found in the minimalist PutA (Fig. 2). The DNA-binding domain (residues 1–49) has a ribbon helix helix (RHH) fold and forms the canonical RHH dimer in solution (9, 19). The other extra domain (CTD, C-terminal domain) has ~ 200 residues and is inserted between the NAD^+ -binding domain and the predicted conserved C-terminal motif. The function of the CTD is unknown.

Although structures of the DNA-binding (9, 19) and PRODH (14, 16, 20–22) domains of EcPutA are known, the three-dimensional structure of a full-length trifunctional PutA has remained elusive since the discovery of PutAs in the late 1970s (23). Here, we report small-angle x-ray scattering (SAXS) studies of EcPutA, which provide the first view of the three-dimensional architecture of a trifunctional PutA.

EXPERIMENTAL PROCEDURES

Expression and Purification of EcPutA—The plasmid used to express EcPutA (pKA8H-EcPutA) was created by subcloning the *putA* gene from a previously described pET-3a vector (11) into pKA8H (kindly provided by Dr. Christopher Hill) using NdeI and BamHI restriction sites. The expressed protein includes the 1320-residue EcPutA with an N-terminal His₈ tag and intervening tobacco etch virus protease (TEVP) cleavage site. Treatment with TEVP results in the native polypeptide preceded by Gly-His.

EcPutA was expressed in *E. coli* using standard methods and purified using immobilized metal affinity chromatography (His-Trap Ni²⁺-Sephacrose HP, GE Healthcare). Fractions eluted from the Ni²⁺-Sephacrose column that contained EcPutA were pooled, and TEVP, 1 M DTT, and 20 \times TEV buffer (1 M Tris-HCl, 10 mM EDTA, pH 8.0) were added so that the resulting solution contained 3 mg of TEVP per 50 mg of EcPutA in 50 mM Tris-HCl, 0.5 mM DTT, and 0.5 mM EDTA, pH 8.0. The sample was incubated for 3 h at 30 °C, dialyzed overnight at 4 °C, and injected onto the Ni²⁺-Sephacrose column. The flow-through was collected, dialyzed into 50 mM Tris-HCl, 50 mM NaCl, 0.5 mM EDTA, 0.5 mM DTT, and 5% glycerol, pH 8.0, and concentrated to 10–25 mg/ml using a centrifugal concentrator. The protein concentration was measured with the bicinchoninic acid method (Pierce kit). Size exclusion chromatography (SEC) was used as the final step of purification. As described by Brown and Wood (24), EcPutA exhibits two apparent species in SEC. The major species is the functional dimeric protein, and the minor species appears to be the isolated subunit. The dimer was isolated using either a Superdex 200 SEC column or a Shodex KW-803 SEC column.

Subcloning and Purification of Domain Deletion Constructs—A domain deletion construct having EcPutA residues 1–1085 (PutA1–1085) was created. The coding sequence for residues 1–1085 was amplified by PCR from a pET-23b plasmid harboring the *putA* gene (25) and subcloned into pET-23b using NdeI and EcoRI restriction sites. PutA1–1085 was purified as described above for EcPutA, except the C-terminal His tag was retained.

Another domain deletion construct having EcPutA residues 86–1320 (PutA86–1320) was also created. The coding sequence for these residues was amplified by PCR from the plasmid pKA8H-EcPutA and subcloned into pKA8H using NdeI and BamHI restriction sites. PutA86–1320 was purified using immobilized metal affinity chromatography followed by cleavage of the affinity tag, passage through the affinity column to remove the tag and uncleaved protein, and finally anion exchange chromatography (HiTrap Q-Sephacrose, GE Healthcare). For the latter step, the loading buffer was 50 mM Tris, 0.5

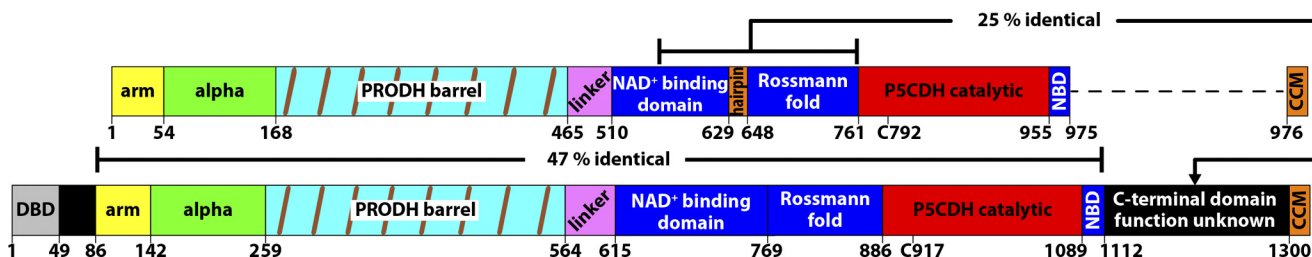


FIGURE 2. Schematic diagram depicting a multiple sequence alignment of minimalist PutAs, represented by BjPutA (top), and trifunctional PutAs, represented by EcPutA (bottom). BjPutA and EcPutA have 999 and 1320 residues, respectively. DBD, DNA-binding domain; NBD, NAD⁺-binding domain; CCM, conserved C-terminal motif.

mM EDTA, and 5% glycerol, pH 8.0, and the protein was eluted with a 0–0.5 M linear NaCl gradient.

Small-angle X-ray Scattering—SAXS experiments were performed at the SIBYLS beamline (12.3.1) of the ALS (26). For each sample, scattering intensities (I) were measured at three protein concentrations to ensure concentration-independent scattering. Exposures of 0.5, 1.0, and 5.0 s were used to check for radiation damage. The scattering curves collected from the protein sample were corrected for background scattering using intensity data collected from the dialysis buffer, SEC effluent, or flow-through from a centrifugal concentrator. Composite scattering curves were generated with PRIMUS (27) by scaling and merging the background-corrected high q region data from the 5.0-s exposure with the low q region data from a shorter exposure (0.5 or 1.0 s). For one of the EcPutA samples, the scattering curves (3.3, 6.7, and 10.0 mg/ml) were extrapolated to zero concentration, and composite scattering curves were generated by scaling and merging the background-corrected high q region data from the 10 mg/ml sample with the low q region zero-extrapolated data. Scattering curves were subjected to indirect Fourier transform using GNOM (28) to yield the pair distribution function ($P(r)$), from which the radius of gyration (R_g) and the maximum particle dimension (D_{max}) were estimated. PRIMUS was used to calculate Porod volumes. The molecular weight in solution was estimated from SAXS data using the relationship, $M = I(0)/Kc$, where M is the molecular weight, $I(0)$ is the intensity extrapolated to zero scattering angle, c is the protein concentration in mg/ml, and K is a constant determined from beamline calibration measurements using glucose isomerase as a standard (29). GASBOR (30) was used to calculate shape reconstructions, and DAMAVER (31) was used to average and filter the resulting dummy atom models. The Situs module `pdb2vol` was used to convert the averaged, filtered models into volumetric maps (32). SUPCOMB was used to superimpose dummy atom models (33).

Rigid Body Modeling Using SAXS Data—Modeling of EcPutA was performed using two rigid bodies: the 1.9-Å resolution crystal structure of the DNA-binding domain dimer (PDB 2GPE) (19) and a hybrid x-ray/homology model of residues 87–1113. The model of residues 87–1113 was built by combining the crystal structure of an EcPutA PRODH domain construct (PutA86–630, PDB code 1TIW) (16) with homology models based on the BjPutA structure (PDB code 3HAZ) generated with I-TASSER (34) and SWISS-MODEL (35). The BjPutA structure is a good template for modeling this part of EcPutA because the two enzymes are 47% identical (62% simi-

lar) in this region (Fig. 2, supplemental Fig. S2). Furthermore, PutA86–630 exhibits the arm, PRODH barrel, and linker domains also found in BjPutA (1.4-Å root mean square deviation). Neither the CTD nor the conserved C-terminal motif was included in rigid body modeling.

The strategy for rigid body modeling was based on the assumption that the DNA-binding domain is essential for dimerization, which follows from the domain deletion studies (see below). This assumption implies that the DNA-binding domain dimer resides in the connector region of the SAXS envelope, whereas residues 87–1113 are located in the large, spatially separated lobes. The EcPutA DNA-binding domain dimer (PDB code 2GPE) was manually fitted into the connector region of the consensus SAXS volumetric map with its 2-fold axis coincident with the 2-fold axis of the SAXS map. The structure fit equally well in two orientations corresponding to the DNA-binding surface facing the concave or convex surfaces of the envelope.

COLORES (36) was used to dock the x-ray/homology model of residues 87–1113 into the lobes. The volumetric maps used for these calculations were created as follows. First, the dummy atoms of the averaged, filtered consensus reconstruction model that overlapped the docked DNA-binding domain dimer were identified manually with PyMol and deleted. The remaining dummy atoms formed two clusters corresponding to the two lobes. These clusters of atoms were saved as two separate coordinate files and converted to volumetric maps, which were used for two COLORES docking calculations.

The poses of the x-ray/homology model of residues 87–1113 from COLORES were combined with the two poses of the docked DNA-binding domain dimer to generate several models, which were then ranked according to the agreement with the experimental scattering profiles using the FoXS χ parameter (37). The linker between residues 47 and 87 was modeled using rapter (38) via `ccp4i` (39). The SAXS volumetric map was input to rapter to constrain the modeled peptide inside the SAXS envelope.

Multiangle Light Scattering—The molecular weight of EcPutA in solution was estimated using a multiangle light scattering (MALS) detector coupled to a Shodex KW-803 SEC column. The MALS analysis was performed in-line to SEC separation using an 18-angle DAWN HELEOS detector (Wyatt Technology) with detector 12 replaced with a DynaPro quasi-elastic light scattering detector. Protein concentrations were simultaneously monitored with an Optilab refractive index detector (Wyatt Technology). System calibrations were per-

formed with glucose isomerase (Hampton Research) dissolved in 50 mM Tris-HCl, 50 mM NaCl, 0.5 mM EDTA, 0.5 mM DTT, and 5% glycerol, pH 8.0. The flow rate was 0.9 ml/min. The molecular weight of PutA86–1320 was estimated similarly using a MALS detector coupled to a G5000PWXL SEC column (Tosoh Bioscience, Montgomeryville, PA). The column buffer was 50 mM Tris-HCl, 50 mM NaCl, 0.5 mM EDTA, 0.5 mM THP, and 5% glycerol, pH 8.0. The flow rate was 0.75 ml/min.

Biochemical Assays—Kinetic parameters for PRODH activity were determined at 25 °C in 100 mM MOPS buffer, pH 8.0, using proline as the substrate (0–500 mM) as previously described (17). P5CDH activity was measured using P5C as the substrate (0–1.5 mM, L-P5C) and 0.2 mM NAD⁺ as previously described (24). NADH formation was monitored at 340 nm, and the extinction coefficient of 6220 M⁻¹ cm⁻¹ for NADH was used to calculate the kinetic parameters. P5C is not commercially available, therefore DL-P5C was chemically synthesized as described (40). DL-P5C was stored in acid at 4 °C. Immediately before performing kinetics experiments DL-P5C was neutralized to pH 6.5–8.0, quantified with *O*-aminobenzaldehyde (forms complex absorbing at 443 nm with $\epsilon = 2590 \text{ M}^{-1} \text{ cm}^{-1}$), and diluted with ice-cold assay buffer to make a stock solution. Due to the limited availability of P5C, the saturation region of the Michaelis-Menten curve was not accessible, which prevented determination of k_{cat} and K_m . Therefore, the ratio of k_{cat} to K_m in the limit of $[S] \ll K_m$ was estimated from the slope of the linear region of the Michaelis-Menten curve at low substrate concentration.

Tryptophan fluorescence quenching was used to study the binding of NAD⁺ to PutA following an approach described previously (41). PutA (0.5–1.0 μM) was excited at 295 nm, and the maximal emission at 335 nm was measured at increasing concentrations of NAD⁺ (0–60 μM). A control assay without protein was performed similarly and used to correct for any inner filter effect. The dissociation constant (K_d) was estimated by fitting the corrected fluorescence quenching data to a single-site binding isotherm. The DNA binding activities of PutA and PutA1–1085 were studied using gel mobility shift assays as previously described (9).

RESULTS

Oligomeric State of EcPutA from SEC-MALS—The oligomeric state of EcPutA in solution was studied using SEC-MALS (Fig. 3A). The data suggest that the purified protein is monodisperse with an apparent molecular mass of 274 ± 3 kDa. This value is within 6% of the predicted molecular mass of 290 kDa for the dimer, in agreement with previous studies (24).

SAXS Analysis of EcPutA—SAXS data from five EcPutA samples differing in the reference buffer used for subtraction or the protein batch are shown in Fig. 4, and parameters derived from SAXS are listed in Table 1. The scattering curves exhibit a perceptible depression near $q = 0.045 \text{ \AA}^{-1}$ and bump near $q = 0.065 \text{ \AA}^{-1}$ (arrows in Fig. 4A). The Guinier plots show good linearity, with R^2 scores greater than 0.994 (Fig. 4A, inset). The $P(r)$ curves exhibit a major peak at 44 \AA and a prominent shoulder peak at 110 \AA (Fig. 4B), which is consistent with a particle having two spatially separated lobes. The maximum particle dimension (D_{max}) is in the range 200–210 \AA . The real space

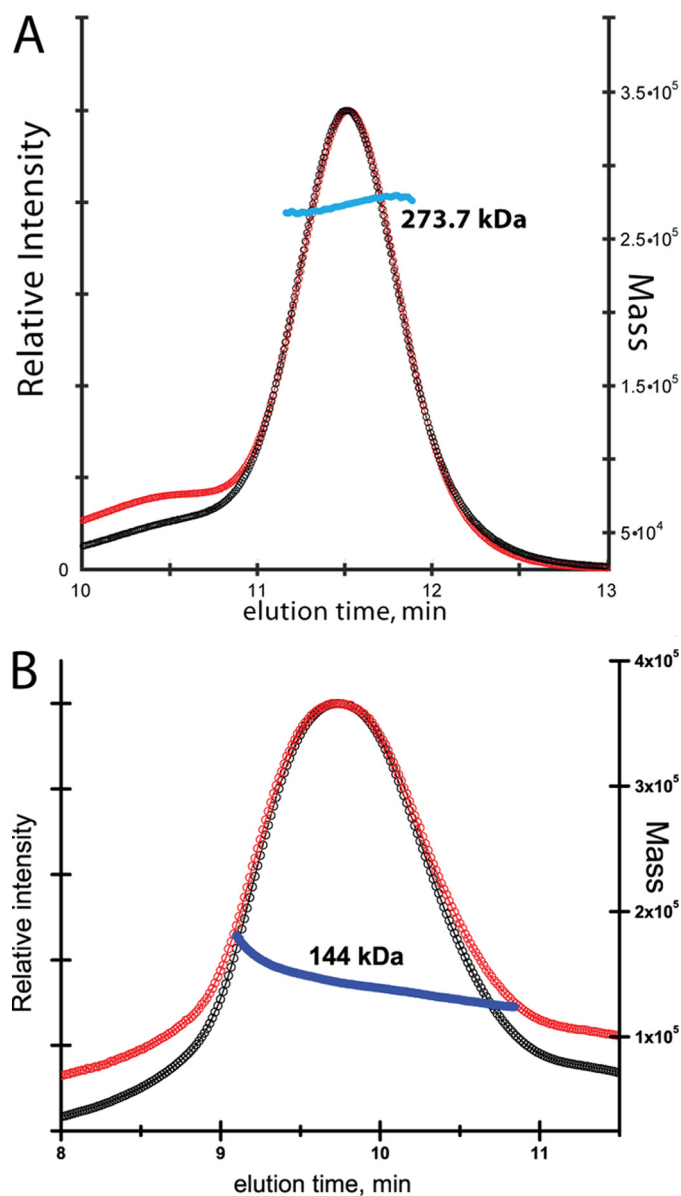


FIGURE 3. Determination of the molecular weight of EcPutA (A) and PutA86–1320 (B) using SEC-MALS. The red curve represents the light scattering response measured at 90°. The black curve represents the response of the refractive index detector. The blue curve shows the derived molecular weight.

radius of gyration (R_g) derived from $P(r)$ calculations spans 62.4–63.3 \AA with an average of $62.8 \pm 0.4 \text{ \AA}$. The $I(0)$ value obtained from a scattering curve that was collected on a calibrated beamline yielded a molecular mass of 285 kDa, consistent with a dimeric protein.

Porod-Debye analysis was performed to assess the flexibility of EcPutA (Fig. 4C). For well folded proteins, a plot of $q^4 I(q)$ versus q^4 restricted to low q reaches an asymptotic value, and the absence of a Porod-Debye plateau suggests that the protein contains substantial regions of unstructured polypeptide (42). Thus, the Porod-Debye plateau is a diagnostic indicator of fold- edness akin to Kratky analysis. The Porod-Debye plots for EcPutA exhibit an obvious plateau, suggesting that the protein is well folded and does not have large regions of unstructured polypeptide (Fig. 4C).

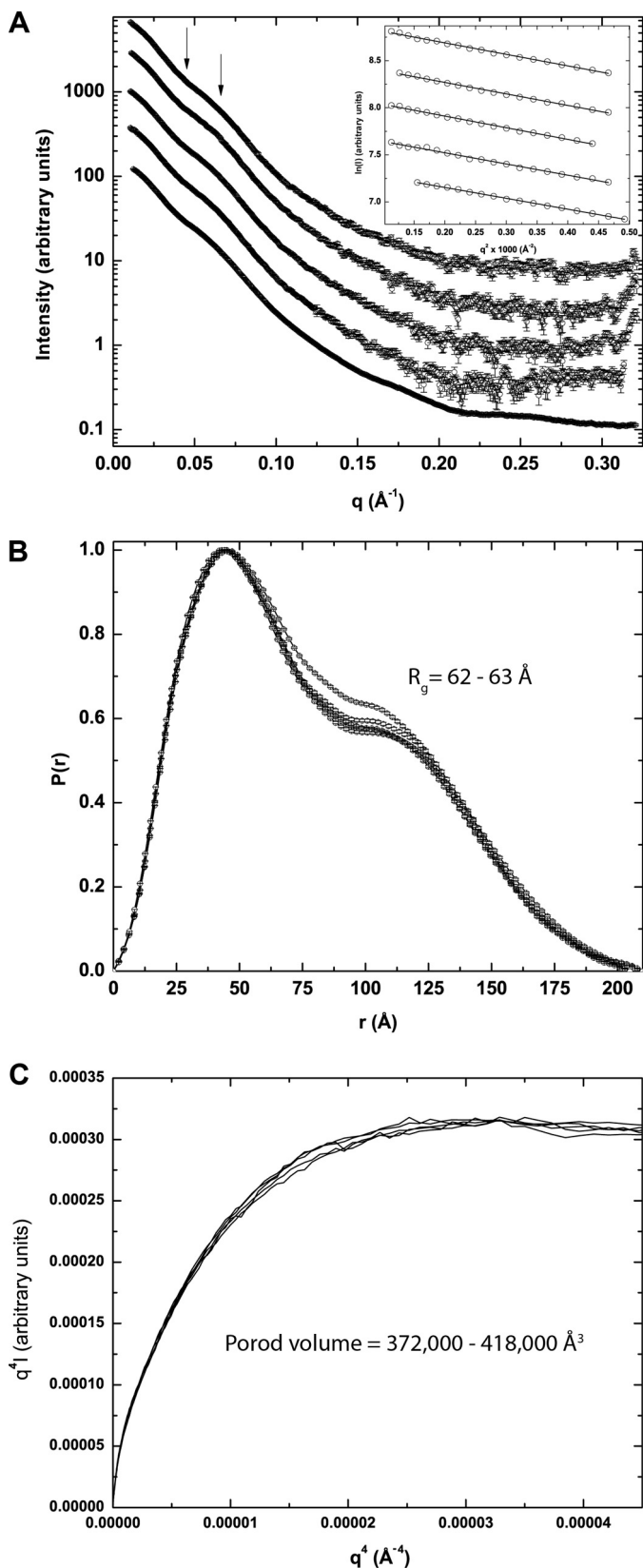


FIGURE 4. SAXS data for five replicate EcPutA samples. *A*, composite scattering curves and Guinier plots (restricted to $qR_g = 0.63$ – 1.3). The arrows mark the depression and bump features at $q = 0.045 \text{ \AA}^{-1}$ and $q = 0.065 \text{ \AA}^{-1}$, respectively, which are characteristic of EcPutA. *B*, $P(r)$ curves. *C*, Porod-Debye plots.

Porod-Debye analysis also provides confirmation of the oligomeric state. The Porod volume estimated from the five data sets is $396,000 \pm 16,000 \text{ \AA}^3$. The assumption of a dimeric protein leads to a value for the protein density of $1.22 \pm 0.05 \text{ g/ml}$. This value is well within the range of 0.9 – 1.5 g/ml obtained in a recent analysis of SAXS data from 31 different proteins (42). In contrast, the assumption of a monomeric or trimeric protein results in density values of 0.6 or 1.8 g/ml , respectively, which are unrealistic for a compact folded protein. The MALS and SAXS data support the hypothesis that EcPutA is a stable, monodisperse dimer in solution.

Shape Reconstructions of EcPutA—The low resolution shape of EcPutA was derived from the SAXS data using the shape reconstruction program GASBOR (Fig. 5). Shape reconstructions were performed for each of the 5 data sets, and a consensus shape was obtained by averaging 10 independent models from each data set. The mean normalized spatial discrepancy of the 50-model reconstruction performed without enforcing symmetry (P1) is 1.60 ± 0.07 . The normalized spatial discrepancy for the P2 consensus model is 1.51 ± 0.08 , thus neither the mean normalized spatial discrepancy nor the variation increased substantially when enforcing 2-fold symmetry. This result is consistent with the fact that the P1 shape exhibits approximate 2-fold symmetry (Fig. 5A).

The reconstructions suggest that EcPutA is a symmetric, V-shaped dimer having dimensions of $205 \times 85 \times 55 \text{ \AA}$ (Fig. 5B). The particle has two large lobes that connect via a short cylindrical section with a diameter of 30 \AA . The molecular shape resembles a curved and slightly twisted dumbbell. The molecular 2-fold axis passes through a connecting cylinder and is perpendicular to the longest axis of the dimer and parallel to the 85 - \AA axis. Thus, the two protein chains presumably meet in the connecting cylinder to form a symmetric dimer interface.

Domain Deletion Analysis—Domain deletion analysis was used to identify the domain(s) involved in dimerization. Two domain deletion mutants were created: PutA1–1085 and PutA86–1320. PutA1–1085 lacks the CTD and the conserved C-terminal motif, whereas PutA86–1320 contains all domains except the DNA-binding domain and the polypeptide that connects the DNA-binding domain to the arm (see Fig. 2).

Enzyme and DNA-binding activities were measured to examine the impacts of the deletions on EcPutA function. Both deletion mutants exhibit PROD H activity similar to that of EcPutA (Table 2). The PROD H kinetic parameters for PutA86–1320 were k_{cat} of $7.5 \pm 0.1 \text{ s}^{-1}$ and K_m of $67 \pm 4 \text{ mM}$ ($k_{\text{cat}}/K_m = 112 \text{ M}^{-1} \text{ s}^{-1}$). Those of PutA1–1085 were k_{cat} of $10.6 \pm 0.2 \text{ s}^{-1}$ and K_m of $122 \pm 5 \text{ mM}$ ($k_{\text{cat}}/K_m = 87 \text{ M}^{-1} \text{ s}^{-1}$). For reference, the PROD H kinetic constants for EcPutA were 7.5 s^{-1} and 100 mM ($k_{\text{cat}}/K_m = 75 \text{ M}^{-1} \text{ s}^{-1}$) (12). The P5CDH activity of PutA86–1320 ($k_{\text{cat}}/K_m = 783 \text{ M}^{-1} \text{ s}^{-1}$) is near that of EcPutA ($1409 \text{ M}^{-1} \text{ s}^{-1}$), but the P5CDH activity of PutA1–1085 was below detection (Table 2). The latter result likely reflects that fact that PutA1–1085 lacks a conserved ~ 20 -residue section of the P5CDH domain (1086–1108, supplemental Fig. S2). To determine whether the loss of P5CDH activity in PutA1–1085 was due to diminished NAD^+ binding, tryptophan fluorescence quenching experiments were performed. The K_d value for NAD^+ binding to PutA1–1085 was $5.5 \pm 2 \text{ \mu M}$, which was

TABLE 1
Parameters derived from SAXS experiments

Sample	R_g^a	D_{max}^b	V_{Porod}^c	Mass ^d	Oligomeric state
EcPutA	\AA	\AA	\AA^3	<i>kDa</i>	
EcPutA	62.8 ± 0.4	200–210	$396,000 \pm 16,000$	285 ± 29	Dimer
PutA1–1085	59.9 ± 0.1	200	345,000	ND ^e	Dimer
PutA86–1320	43.2 ± 0.1	165	186,000	140 ± 14	Monomer

^a The real space radius of gyration was estimated from calculations of $P(r)$ using GNOM. The uncertainty for EcPutA is the S.D. from five replicate samples. The uncertainties for PutA1–1085 and PutA86–1320 were obtained from single $P(r)$ calculations.

^b The maximum particle dimension was estimated from calculations of $P(r)$ using GNOM. The range listed for EcPutA is based on five replicate samples.

^c The Porod volume was calculated using PRIMUS. The uncertainty for EcPutA is the S.D. from five replicate samples.

^d The molecular mass was determined from $I(0)$, which was calibrated using glucose isomerase as a standard. The protein concentration was 3.3 mg/ml for EcPutA and 9 mg/ml for PutA86–1320. The quoted uncertainty of 10% is from Mylonas and Svergun (29).

^e Not determined because the concentration of this sample was not measured prior to SAXS analysis.

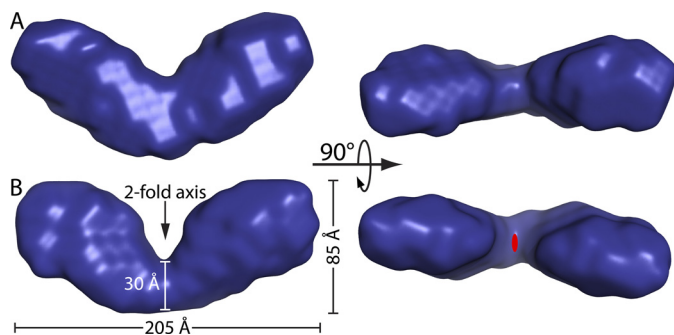


FIGURE 5. Consensus shape reconstructions for EcPutA calculated using GABSOR assuming P1 (A) and P2 (B) symmetries. Each surface represents the averaged, filtered volume based on 10 independent models from each of five samples (50 models total). Two orthogonal views of each shape are shown. The oval in panel B (right) represents the 2-fold axis of the envelope.

TABLE 2
Kinetic parameters for EcPutA and domain deletion mutants

	PRODH activity			P5CDH activity,
	k_{cat}	K_m	k_{cat}/K_m	k_{cat}/K_m
	s^{-1}	<i>mM</i>	$M^{-1}s^{-1}$	$M^{-1}s^{-1}$
EcPutA ^a	7.5^a	100^a	75^a	1410 ± 31
PutA1–1085	10.6 ± 0.2	122 ± 5	87 ± 4	BD ^b
PutA86–1320	7.5 ± 0.1	67 ± 4	112 ± 7	783 ± 57

^a From Vinod *et al.* (12).

^b Below the detection limit of 0.03 μM NADH/min.

similar to that of EcPutA ($2.6 \pm 0.2 \mu M$), demonstrating that the NAD^+ -binding domain was functional in PutA1–1085. Finally, the DNA-binding activity of PutA1–1085 was comparable with that of EcPutA, as demonstrated by gel mobility shift assays (supplemental Fig. S3). In summary, the domain deletion mutants exhibit the expected activities.

The SAXS curve for PutA1–1085 is very similar to that of EcPutA (Fig. 6A). In particular, the curve exhibits the depression and bump at $q = 0.045 \text{ \AA}^{-1}$ and $q = 0.065 \text{ \AA}^{-1}$, respectively, which are characteristic of the full-length, dimeric protein. The $P(r)$ curve for PutA1–1085 is strikingly similar to that of EcPutA (Fig. 6B). The R_g value was 60 \AA , which is comparable with the value of 63 \AA for EcPutA. Porod-Debye plots for PutA1–1085 exhibit a well defined plateau resulting in a Porod volume of $345,000 \text{ \AA}^3$ (Fig. 6C), which is just 13% smaller than that of EcPutA. These results suggest that PutA1–1085 is dimeric in solution.

The scattering curve for PutA86–1320 is noticeably different from that of EcPutA (Fig. 6A). In particular, the characteristic features observed in EcPutA SAXS curves at $q = 0.045 \text{ \AA}^{-1}$ and $q = 0.065 \text{ \AA}^{-1}$ are absent. The $P(r)$ function shows a more profound difference, exhibiting just a single maximum near 41

\AA (Fig. 6B). The R_g of PutA86–1320 is 43 \AA , which is 20 \AA smaller than that of EcPutA. Also, the maximum particle dimension is $\sim 165 \text{ \AA}$, which is about 40 \AA shorter than that of EcPutA. The estimated Porod volume for PutA86–1320 is $186,000 \text{ \AA}^3$, which is about one-half of the volume of EcPutA. The molecular mass estimated from $I(0)$ is $140 \pm 14 \text{ kDa}$, which is within 4% of expected monomer molecular mass of 134 kDa (Table 1). Furthermore, analysis of PutA86–1320 using SEC-MALS suggests a molecular mass in solution of 144 kDa (Fig. 3B). These data are consistent with PutA86–1320 being monomeric.

In summary, domain deletion analysis suggests that residues 1086–1320 are not essential for dimerization, and that an essential dimerization domain is located within residues 1–85. We suggest that the DNA-binding domain (residues 1–47) is the essential dimerization domain, because RHH domains bind DNA as obligate dimers (43). Furthermore, the DNA-binding domain of EcPutA has been expressed as an isolated protein (PutA52) and shown to form the classic RHH dimer in solution (9, 19).

Rigid Body Modeling—Rigid body modeling was performed to generate hypotheses about the spatial arrangement of domains in the EcPutA dimer. Two rigid bodies were used: the 1.9-\AA resolution crystal structure of the DNA-binding domain dimer (PDB 2GPE, Fig. 7A, left) and a hybrid x-ray/homology model of residues 87–1113 (Fig. 7A, right). As described under “Experimental Procedures,” the strategy used for modeling was based on the assumption that the DNA-binding domain is located in the connector section of the SAXS envelope with its 2-fold axis coincident with that of the envelope. This assumption is consistent with the domain deletion results, which show that the DNA-binding domain is essential for dimerization. Consequently, the catalytic units (residues 87–1113) correspond to the two large lobes of the envelope.

The best model (model 1), as judged by the lowest χ value from FoXS, is shown in Fig. 7B. Model 1 shows good agreement with the experimental scattering profiles (Fig. 7C). Note that the model curve exhibits the characteristic depression near $q = 0.045 \text{ \AA}^{-1}$ and bump near $q = 0.065 \text{ \AA}^{-1}$. The χ values calculated from FoXS for the fits to the five experimental curves are in the range of 2.0–5.2 over the entire q range. The fit is remarkably good, considering that 208 of the 1320 residues are missing in the homology model. These results suggest that, at this resolution, the shape of the rigid body model is close to that of the full-length enzyme and that the additional missing residues are

SAXS Studies of Trifunctional PutA

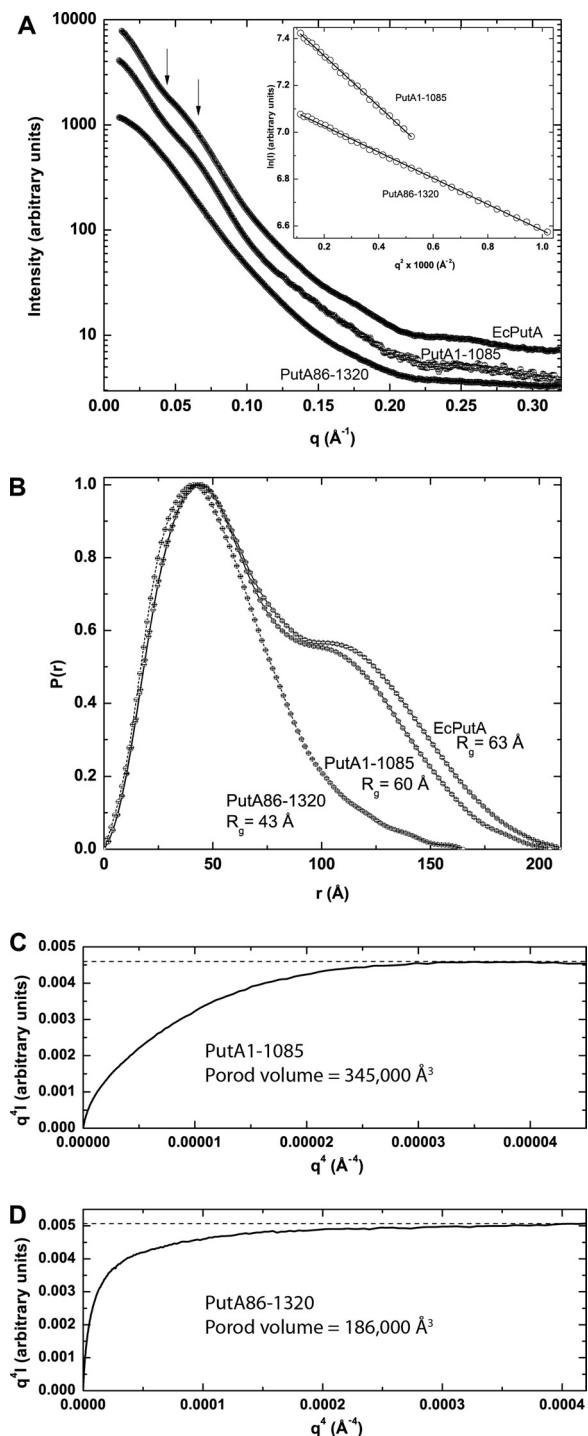


FIGURE 6. SAXS analysis of EcPutA domain deletion mutants PutA1-1085 and PutA86-1320. *A*, composite scattering curves and Guinier plots (restricted to $qR_g = 0.61-1.3$ for PutA1-1085 and $qR_g = 0.43-1.3$ for PutA86-1320). The linear fits of the Guinier plots have $R^2 = 0.999$ for both proteins. The arrows mark $q = 0.045 \text{ \AA}^{-1}$ and $q = 0.065 \text{ \AA}^{-1}$. *A* scattering curve for EcPutA is shown for reference. *B*, $P(r)$ curves for the domain deletion mutants and EcPutA. *C*, Porod-Debye plot for PutA1-1085. *D*, Porod-Debye plot for PutA86-1320.

packed against the structure as opposed to extending into solution.

Several features of the model are notable. The catalytic units are oriented with the PRODH half of the polypeptide chain near the DNA-binding domain and the P5CDH half in the outer-

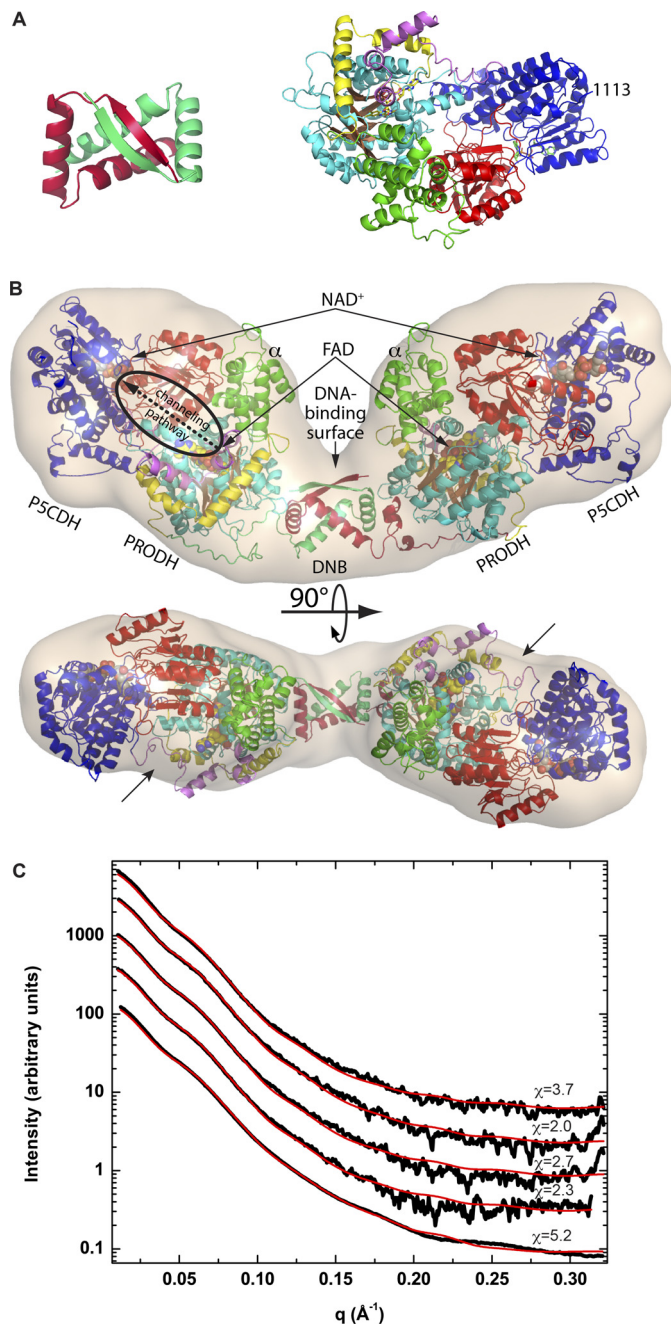


FIGURE 7. Rigid body model 1 of EcPutA. *A*, crystal structure of the DNA-binding domain dimer (left, PDB code 2GPE) and a hybrid x-ray/homology model for residues 87-1113 (right). The model of 87-1113 has the same orientation as the BjPutA protomer under [supplemental Fig. S1A](#). Note that this model is essentially identical to the BjPutA protomer, except the oligomerization flap is absent. The domains are colored according to the domain diagrams in Fig. 2. *B*, two views of the current working model of EcPutA. The locations of the PRODH, α , and P5CDH domains are noted in the upper panel. The dashed oval shows the location of the putative substrate-channelling cavity. As modeled, the cavity is open to bulk solvent. The arrows in the lower panel indicate possible locations of the CTD. *C*, comparison of the five experimental SAXS curves for EcPutA (black) and the theoretical curve calculated from model 1 using FoXS (red). The FoXS χ value is listed for each curve.

most part of the lobe. Residues 47 and 87 are located on the same face of the envelope and separated by 44 Å, which is close enough to be connected by 39 residues. The α domains line the trench between the two lobes and face each other at a distance of 40 Å. A consequence of the large separation

between the two catalytic units is that the putative substrate-channeling cavity is open to the bulk medium (*dashed oval* in Fig. 7B).

Other models generated by the COLORES docking calculations were examined to test the reliability of model 1. The top two of these alternative models, as judged by the fit to the experimental scattering profiles, are shown in [supplemental Fig. S4](#). In model 2 ($\chi = 3.2\text{--}10.2$ for the five replicate EcPutA SAXS curves) COLORES positioned the catalytic units such that the α domains face the convex surface of the envelope. With the catalytic units in this orientation, the DNA-binding surface is constrained to also face the convex side of the envelope for residues 47 and 87 to be connected by the intervening 39 residues. Thus, the DNA-binding domain dimer was manually rotated by 180° from that of model 1. Model 3 ($\chi = 4.0\text{--}9.1$) is different from models 1 and 2 in that the P5CDH domains are near the DNA-binding domains, whereas the PRODH domains are in the distal ends of the lobes. Although models 2 and 3 have satisfactory agreement with the consensus SAXS shape, the fits to the scattering profiles are substantially worse than that of model 1. Thus, the experimental SAXS data are sufficiently sensitive to rule out models having domain orientations that are substantially different from those of model 1.

DISCUSSION

The oligomeric states and quaternary structures of PutAs are not conserved. To date, the oligomeric states of just two PutAs have been determined using rigorous biophysical methods. Almost 20 years ago, Brown and Wood (24) used sedimentation and light scattering to show that EcPutA forms a dimer in solution. We confirmed this result using MALS and SAXS. Last year, we reported SAXS and equilibrium sedimentation data showing that BjPutA, a minimalist bifunctional PutA, forms a ring-shaped, dimer-of-dimers tetramer having 222 symmetry (18). Thus, despite nearly 50% amino acid sequence identity, these two PutAs have different oligomeric states.

Considering the high identity between EcPutA and BjPutA, one might hypothesize that the EcPutA dimer resembles one of the three 2-body assemblies of the BjPutA tetramer. However, the R_g values of those assemblies are 44.8, 44.3, and 47.5 Å, which are much smaller than the R_g of 63 Å for EcPutA. Furthermore, the P(r) curves calculated from the BjPutA assemblies are distinctly different from that of EcPutA ([supplemental Fig. S5](#)). In particular, the distributions of vectors in the BjPutA dimers lack the prominent shoulder at 110 Å, suggesting that the catalytic units are farther apart in EcPutA than in BjPutA. In fact, if two BjPutA protomers are separated as in rigid body model 1, the resulting P(r) exhibits the characteristic bimodal shape of EcPutA ([supplemental Fig. S5, dashed curve](#)). We thus conclude that neither the oligomeric state nor the quaternary structure are conserved in the PutA family.

This lack of conservation perhaps makes sense considering the additional function of EcPutA as a transcriptional repressor, which requires dimerization of the DNA-binding domain. Indeed, the DNA-binding domain was found here to be essential for dimerization of EcPutA. The connecting cylinder of the SAXS envelope accommodates the RHH dimer, but is not large enough to fit additional domains, suggesting that the DNA-

binding domain is the sole dimerization domain. Thus, it appears that function trumps homology in determining the oligomeric state and quaternary structure of PutA.

DNA is predicted to bind in the trench on the concave surface of the protein ([supplemental Fig. S6](#)). The model is consistent with structural data on EcPutA-DNA association. In particular, side chains of the RHH domain that are known to contact DNA (9) are solvent exposed in the SAXS model. These critical residues are located in the β -strand (residues 5, 7, and 9) and N terminus of the second helix of the RHH-fold (residues 28–30). The model suggests the hypothesis that elements outside of the RHH domain, such as residues in α domain and PRODH barrel, may influence DNA binding. The SAXS model also provides new insights into the redox-dependent transcriptional regulation of the *putA* and *putP* genes by EcPutA. The 419-bp *put* control DNA region was previously shown to have five operator sites, with two of the operators (sites 3 and 4) separated by only one nucleotide (9). The mode of DNA binding predicted in our model ([supplemental Fig. S6](#)) suggests that PutA binding to sites 3 or 4 preclude binding at the neighboring operator sequence. Thus, PutA most likely binds only four operator sites at one time to repress transcription of the *putA* and *putP* genes.

Consideration of the SAXS data in the context of existing biochemical and biophysical data on EcPutA provides a new model for gene regulation by EcPutA. Previous studies showed that reduction of the FAD causes just a 2-fold increase in the dissociation constant of PutA with *put* control DNA (11), indicating that the FAD redox state has little influence on the intrinsic affinity of EcPutA for DNA. On the other hand, reduction of FAD increases the binding constant for membrane association by several orders of magnitude (15). Essentially, oxidized EcPutA has negligible affinity for the membrane, whereas the reduced protein exhibits nanomolar affinity. Two studies have shown that membrane binding and DNA binding are mutually exclusive (15, 44). Finally, limited proteolysis and Trp fluorescence studies of EcPutA showed that FAD reduction induces a conformational change in the α domain, implying that reduction of the flavin triggers a global conformational change involving, in part, the α domain, that causes EcPutA to switch from being a transcriptional repressor to membrane-bound enzyme (13, 17).

A new model of gene regulation that is consistent with these observations and the SAXS model is that the DNA-binding and membrane-association interfaces are located on the same face of the protein, and that in the oxidized state, the former interface is exposed, whereas the latter is concealed. Reduction of FAD induces a conformational change that exposes the high affinity membrane-binding interface *without* disrupting the DNA-binding interface. The unveiling of the membrane-binding interface drives EcPutA to the membrane surface, which hides the DNA-binding interface from the *put* regulon thereby activating gene transcription. In SAXS model 1, the DNA-binding interface and both α domains are located on the same face of the protein, *i.e.* the concave face (Fig. 7B). We thus hypothesize that the concave face of EcPutA supports both DNA- and membrane-binding, enabling a cloaking mechanism of gene regulation.

The SAXS model also provides insight into the nature of the global conformational changes associated with functional switching. The V-shape of oxidized EcPutA suggests hinge bending analogous to the ν_2 normal mode of water as a natural degree of freedom. Bending in one direction (closing) brings the α domains closer together and narrows the DNA-binding trench, resulting in a less elongated particle. Hinge bending in the opposite direction (opening) extends and flattens the dimer. Whether reduction of the FAD closes or opens the hinge is difficult to predict, but it may be possible to distinguish between these two general models for redox-linked conformational change using SAXS of reduced EcPutA and fluorescence resonance energy transfer of labeled EcPutA.

Spatial separation of the P5CDH domains, as in our rigid body models, is unprecedented in the aldehyde dehydrogenase (ALDH) gene superfamily. The superfamily includes NAD(P)⁺-dependent enzymes catalyzing the oxidation of a variety of aldehyde substrates to their corresponding carboxylic acids (45, 46). P5CDHs belong to the ALDH4 family. Crystal structures of several ALDHs are known (47–49). All feature a 3-domain tertiary structure consisting of a Rossmann-like cofactor-binding domain (also called the N domain), a catalytic domain that furnishes the reactive Cys (also called the C domain), and an oligomerization flap domain formed by a β -hairpin and C-terminal β -strand. BjPutA and the monofunctional P5CDH from *Thermus thermophilus* (50) exhibit this defining architecture. The known structures also show that ALDHs form a domain-swapped dimer in which the oligomerization domain of one protomer interacts with the catalytic domain of the other protomer as in [supplemental Fig. S1C](#). In some ALDHs, the domain-swapped dimers assemble to form tetramers (48, 49) or hexamers (50).

The domain deletion and SAXS data suggest that dimerization of EcPutA is *not* mediated by traditional ALDH oligomerization flap domains. Although unprecedented in the ALDH superfamily, this result is consistent with multiple sequence alignments. In particular, the alignments clearly show that the β -hairpin of the minimalist PutA (residues 633–648) is truncated in trifunctional PutAs ([supplemental Fig. S2, orange box](#)). Consequently, we hypothesize that the ALDH domains of trifunctional PutAs do not have the traditional dimerization flap seen in other ALDHs. Rather, our results suggest that trifunctional PutAs are unique members of the ALDH superfamily because of their mode of dimerization.

Finally, our results provide insight into the function of the CTD. The observation that PutA1–1085 is dimeric suggests that the CTD is not involved in dimerization. Remote homology detection analysis suggests that the CTD is homologous to the Rossmann domain of ALDHs. For example, HHSearch (35) identifies 33 ALDHs with probability scores of 99.1–99.9%, with the top match being BjPutA (probability = 99.9%, *E*-value = $7.7E-26$). The alignment shows that the CTD of EcPutA is 25% identical to residues 551–761 of BjPutA (Fig. 2). Of particular note is the prediction that CTD residues 1175–1190 ([supplemental Fig. S2, green box](#)) form an ALDH β -hairpin homologous to the one found in BjPutA residues 633–648. As noted above, the substrate channeling cavity is open to the bulk medium in the SAXS models, which is inconsistent with

the observation that PutAs exhibit several kinetic signatures of substrate channeling (18, 51).³ These results suggest the hypothesis that the CTD occupies the vacant space in the SAXS envelope between the two active sites (*arrows in lower part of Fig. 7B*), thereby forming an intramolecular lid analogous to the intermolecular lid of BjPutA. Future studies will be needed to test this, and other, hypotheses raised by the model of EcPutA proposed here.

Acknowledgments—We thank Kevin Dyer of the SIBYLS Mail In SAXS Program for collecting some of the SAXS data. We also thank Prof. Krishna K. Sharma for use of his SEC-MALS instrument, and Dr. Santhoshkumar Puttur for helping with SEC-MALS data collection and analysis. Part of this research was performed at the Advanced Light Source. The Advanced Light Source is supported by the Director, Office of Science, Office of Basic Energy Sciences, of the United States Department of Energy under Contract DE-AC02-05CH11231.

REFERENCES

1. Tanner, J. J. (2008) *Amino Acids* **35**, 719–730
2. Zhou, Y., Zhu, W., Bellur, P. S., Rewinkel, D., and Becker, D. F. (2008) *Amino Acids* **35**, 711–718
3. Menzel, R., and Roth, J. (1981) *J. Mol. Biol.* **148**, 21–44
4. Maloy, S. R., and Roth, J. R. (1983) *J. Bacteriol.* **154**, 561–568
5. Wood, J. M. (1987) *Proc. Natl. Acad. Sci. U.S.A.* **84**, 373–377
6. Ostrovsky de Spicer, P., and Maloy, S. (1993) *Proc. Natl. Acad. Sci. U.S.A.* **90**, 4295–4298
7. Muro-Pastor, A. M., and Maloy, S. (1995) *J. Biol. Chem.* **270**, 9819–9827
8. Vilchez, S., Manzanera, M., and Ramos, J. L. (2000) *Appl. Environ. Microbiol.* **66**, 5221–5225
9. Zhou, Y., Larson, J. D., Bottoms, C. A., Arturo, E. C., Henzl, M. T., Jenkins, J. L., Nix, J. C., Becker, D. F., and Tanner, J. J. (2008) *J. Mol. Biol.* **381**, 174–188
10. Brown, E. D., and Wood, J. M. (1993) *J. Biol. Chem.* **268**, 8972–8979
11. Becker, D. F., and Thomas, E. A. (2001) *Biochemistry* **40**, 4714–4721
12. Vinod, M. P., Bellur, P., and Becker, D. F. (2002) *Biochemistry* **41**, 6525–6532
13. Zhu, W., and Becker, D. F. (2003) *Biochemistry* **42**, 5469–5477
14. Lee, Y. H., Nadaraja, S., Gu, D., Becker, D. F., and Tanner, J. J. (2003) *Nat. Struct. Biol.* **10**, 109–114
15. Zhang, W., Zhou, Y., and Becker, D. F. (2004) *Biochemistry* **43**, 13165–13174
16. Zhang, M., White, T. A., Schuermann, J. P., Baban, B. A., Becker, D. F., and Tanner, J. J. (2004) *Biochemistry* **43**, 12539–12548
17. Zhu, W., and Becker, D. F. (2005) *Biochemistry* **44**, 12297–12306
18. Srivastava, D., Schuermann, J. P., White, T. A., Krishnan, N., Sanyal, N., Hura, G. L., Tan, A., Henzl, M. T., Becker, D. F., and Tanner, J. J. (2010) *Proc. Natl. Acad. Sci. U.S.A.* **107**, 2878–2883
19. Larson, J. D., Jenkins, J. L., Schuermann, J. P., Zhou, Y., Becker, D. F., and Tanner, J. J. (2006) *Protein Sci.* **15**, 2630–2641
20. Zhang, W., Zhang, M., Zhu, W., Zhou, Y., Wanduragala, S., Rewinkel, D., Tanner, J. J., and Becker, D. F. (2007) *Biochemistry* **46**, 483–491
21. Ostrander, E. L., Larson, J. D., Schuermann, J. P., and Tanner, J. J. (2009) *Biochemistry* **48**, 951–959
22. Srivastava, D., Zhu, W., Johnson, W. H., Jr., Whitman, C. P., Becker, D. F., and Tanner, J. J. (2010) *Biochemistry* **49**, 560–569
23. Ratzkin, B., and Roth, J. (1978) *J. Bacteriol.* **133**, 744–754
24. Brown, E. D., and Wood, J. M. (1992) *J. Biol. Chem.* **267**, 13086–13092
25. Zhu, W., Gincherman, Y., Docherty, P., Spilling, C. D., and Becker, D. F. (2002) *Arch. Biochem. Biophys.* **408**, 131–136
26. Hura, G. L., Menon, A. L., Hammel, M., Rambo, R. P., Poole, F. L., 2nd, Tsutakawa, S. E., Jenney, F. E., Jr., Classen, S., Frankel, K. A., Hopkins, R. C.,

³ D. F. Becker, unpublished results.

- Yang, S. J., Scott, J. W., Dillard, B. D., Adams, M. W., and Tainer, J. A. (2009) *Nat. Methods* **6**, 606–612
27. Konarev, P. V., Volkov, V. V., Sokolova, A. V., Koch, M. H., and Svergun, D. I. (2003) *J. Appl. Crystallogr.* **36**, 1277–1282
28. Svergun, D. I. (1992) *J. Appl. Crystallogr.* **25**, 495–503
29. Mylonas, E., and Svergun, D. I. (2007) *J. Appl. Crystallogr.* **40**, s245–s249
30. Svergun, D. I., Petoukhov, M. V., and Koch, M. H. (2001) *Biophys. J.* **80**, 2946–2953
31. Volkov, V. V., and Svergun, D. I. (2003) *J. Appl. Crystallogr.* **36**, 860–864
32. Wriggers, W. (2010) *Biophys. Rev.* **2**, 21–27
33. Kozin, M. B., and Svergun, D. I. (2001) *J. Appl. Crystallogr.* **34**, 33–41
34. Zhang, Y. (2008) *BMC Bioinformatics* **9**, 40
35. Arnold, K., Bordoli, L., Kopp, J., and Schwede, T. (2006) *Bioinformatics* **22**, 195–201
36. Chacón, P., and Wriggers, W. (2002) *J. Mol. Biol.* **317**, 375–384
37. Schneidman-Duhovny, D., Hammel, M., and Sali, A. (2010) *Nucleic Acids Res.* **38**, W540–544
38. de Bakker, P. I., DePristo, M. A., Burke, D. F., and Blundell, T. L. (2003) *Proteins* **51**, 21–40
39. Potterton, E., Briggs, P., Turkenburg, M., and Dodson, E. (2003) *Acta Crystallogr. D Biol. Crystallogr.* **59**, 1131–1137
40. Williams, I., and Frank, L. (1975) *Anal. Biochem.* **64**, 85–97
41. Easley, K. E., Sommer, B. J., Boanca, G., Barycki, J. J., and Simpson, M. A. (2007) *Biochemistry* **46**, 369–378
42. Rambo, R. P., and Tainer, J. A. (2011) *Biopolymers* **95**, 559–571
43. Schreiter, E. R., and Drennan, C. L. (2007) *Nat. Rev. Microbiol.* **5**, 710–720
44. Muro-Pastor, A. M., Ostrovsky, P., and Maloy, S. (1997) *J. Bacteriol.* **179**, 2788–2791
45. Sophos, N. A., and Vasiliou, V. (2003) *Chem. Biol. Interact.* **143–144**, 5–22
46. Yoshida, A., Rzhetsky, A., Hsu, L. C., and Chang, C. (1998) *Eur. J. Biochem.* **251**, 549–557
47. Liu, Z. J., Sun, Y. J., Rose, J., Chung, Y. J., Hsiao, C. D., Chang, W. R., Kuo, I., Perozich, J., Lindahl, R., Hempel, J., and Wang, B. C. (1997) *Nat. Struct. Biol.* **4**, 317–326
48. Moore, S. A., Baker, H. M., Blythe, T. J., Kitson, K. E., Kitson, T. M., and Baker, E. N. (1998) *Structure* **6**, 1541–1551
49. Steinmetz, C. G., Xie, P., Weiner, H., and Hurley, T. D. (1997) *Structure* **5**, 701–711
50. Inagaki, E., Ohshima, N., Takahashi, H., Kuroishi, C., Yokoyama, S., and Tahirov, T. H. (2006) *J. Mol. Biol.* **362**, 490–501
51. Surber, M. W., and Maloy, S. (1998) *Arch. Biochem. Biophys.* **354**, 281–287

SUPPLEMENTAL DATA

Small-Angle X-ray Scattering Studies of the Oligomeric State and Quaternary Structure of the Trifunctional Proline Utilization A (PutA) Flavoprotein from *Escherichia coli**

Ranjan K. Singh¹, John D. Larson¹, Weidong Zhu², Robert P. Rambo³, Greg L. Hura³, Donald F. Becker², and John J. Tanner^{1,4}

From the Departments of ¹Chemistry and ⁴Biochemistry, University of Missouri-Columbia, Columbia, MO, 65211, the ²Department of Biochemistry, University of Nebraska-Lincoln, Lincoln, NE 68588, and ³Lawrence Berkeley National Laboratory, Berkeley, CA 94720, USA

Address correspondence to: John J. Tanner, Department of Chemistry, University of Missouri-Columbia, Columbia, MO 65211, USA. Phone: 573-884-1280. Fax: 573-882-2754. E-mail: tannerjj@missouri.edu.

Table of Contents

Fig. S1. Structure of the minimalist PutA, BjPutA.	S-2
Fig. S2. Global sequence alignment of BjPutA and EcPutA	S-3
Fig. S3. Gel-mobility shift assay of EcPutA and PutA1-1085.	S-5
Fig. S4. Two alternative models of EcPutA.	S-6
Fig. S5. Comparison of an experimental P(r) curve for EcPutA with theoretical curves calculated from the BjPutA tetramer.	S-7
Fig. S6. Model of DNA bound to SAXS model 1	S-8

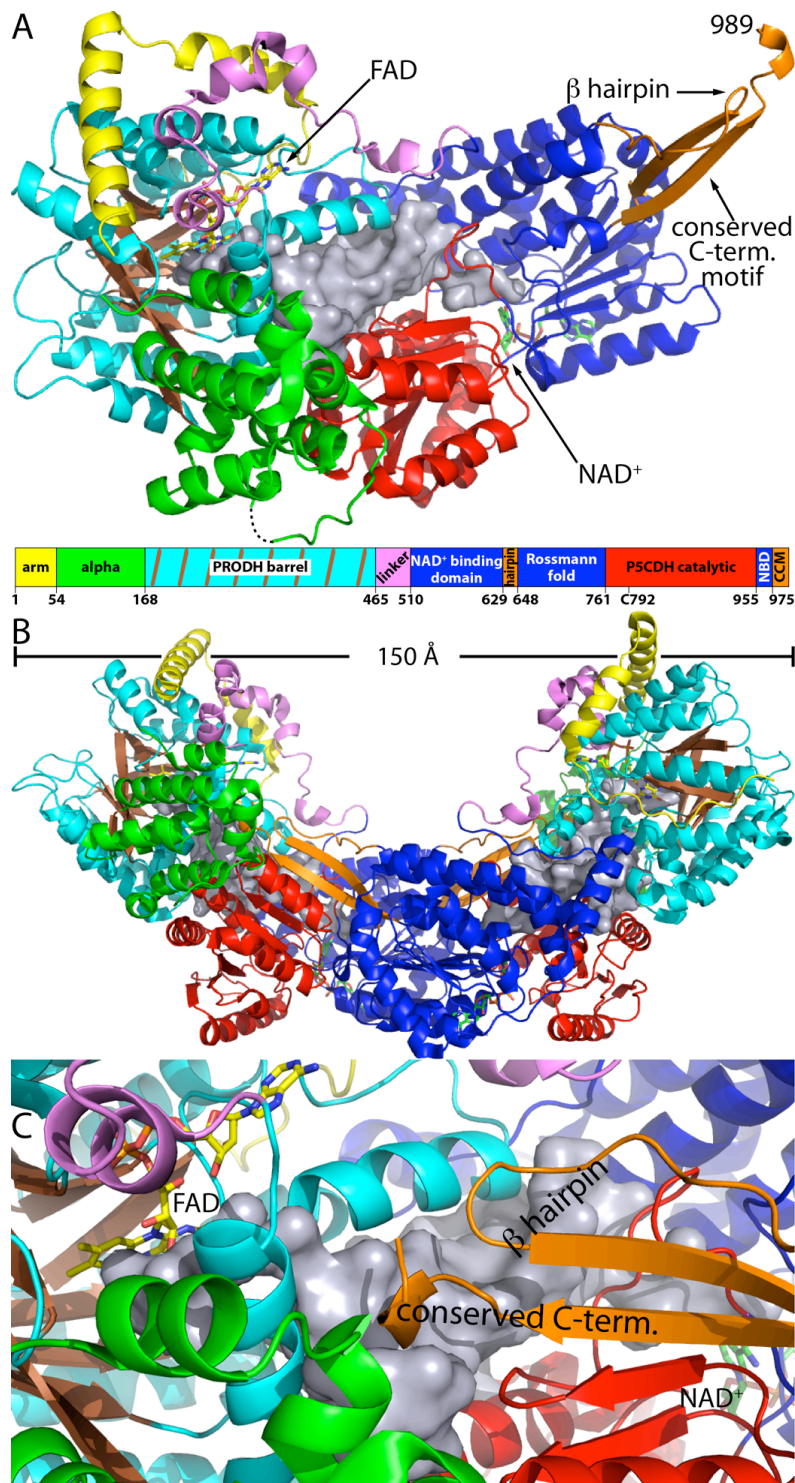


Fig. S1. Structure of the minimalist PutA, BjPutA. (A) Structure of the protomer with the domains colored according to the domain diagram. FAD and NAD⁺ are drawn as sticks in yellow and green, respectively. Abbreviations used in the domain diagram: NBD, NAD⁺-binding domain; CCM, conserved C-terminal motif. (B) Structure of the domain-swapped dimer. (C) Close-up view of the dimer interface highlighting how the β -flap (orange) of one protomer seals the substrate-channeling cavity of the other protomer of the dimer.

AAB59985.1). The secondary structure elements above the sequence are from the BjPutA structure (PDB code 3haz). The secondary structure elements below the sequence for the N-terminal ribbon-helix-helix domain are from a structure of the EcPutA DNA-binding domain (PDB code 2GPE). The star denotes the catalytic Cys of the P5CDH catalytic domain. The orange box denotes the β -hairpin of BjPutA, which is abbreviated in EcPutA. The green box denotes the β -hairpin of EcPutA predicted by remote homology detection. The blue box denotes the conserved C-terminal motif shared by minimalist and trifunctional PutAs.

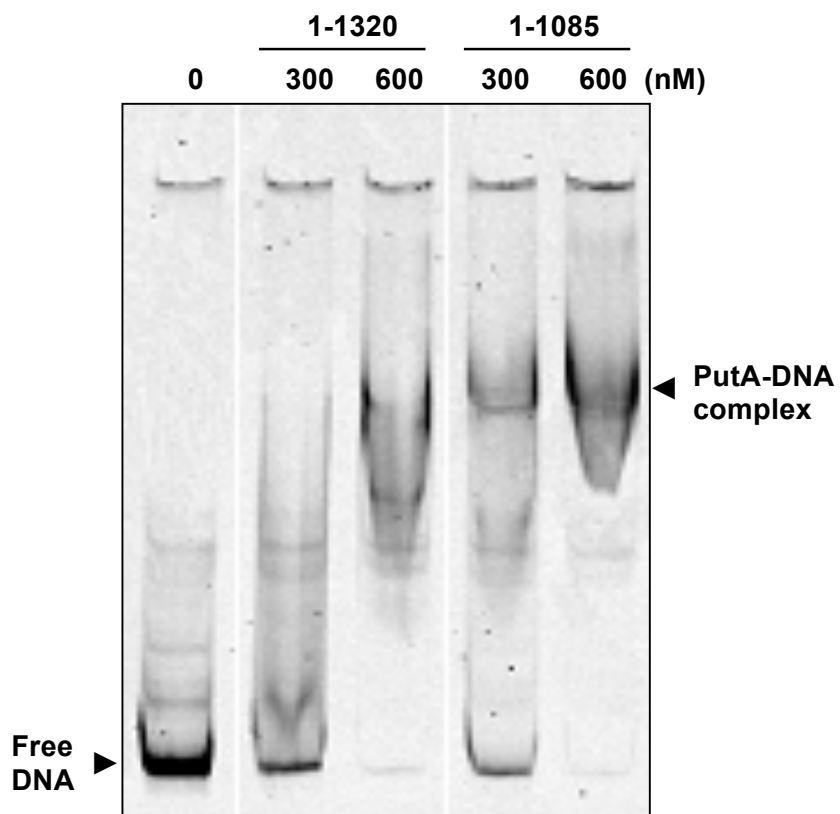


Fig. S3. Gel-mobility shift assay of EcPutA and PutA1-1085. Two different concentrations of EcPutA and PutA1-1085 were added to binding mixtures containing IRdye-700 labeled *E. coli put* intergenic DNA (2 nM) and 100 $\mu\text{g}/\text{mL}$ of nonspecific calf thymus DNA at 23°C.

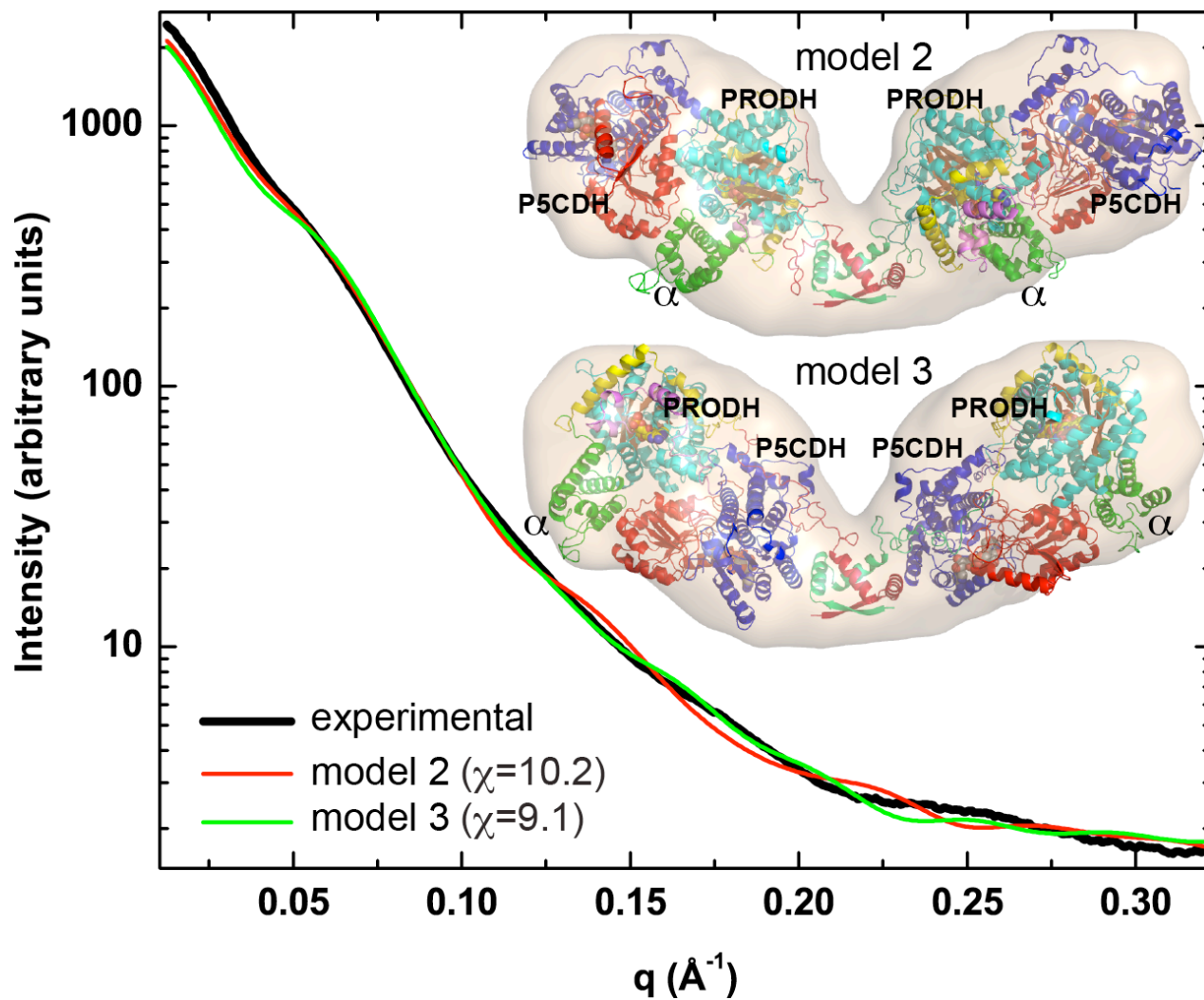


Fig. S4. Two alternative models of EcPutA. Locations of the PRODH, α , and P5CDH domains are indicated. The FoXS χ value is listed for each model. Note that these values (10.2, 9.1) are substantially higher than that of model 1 (5.2).

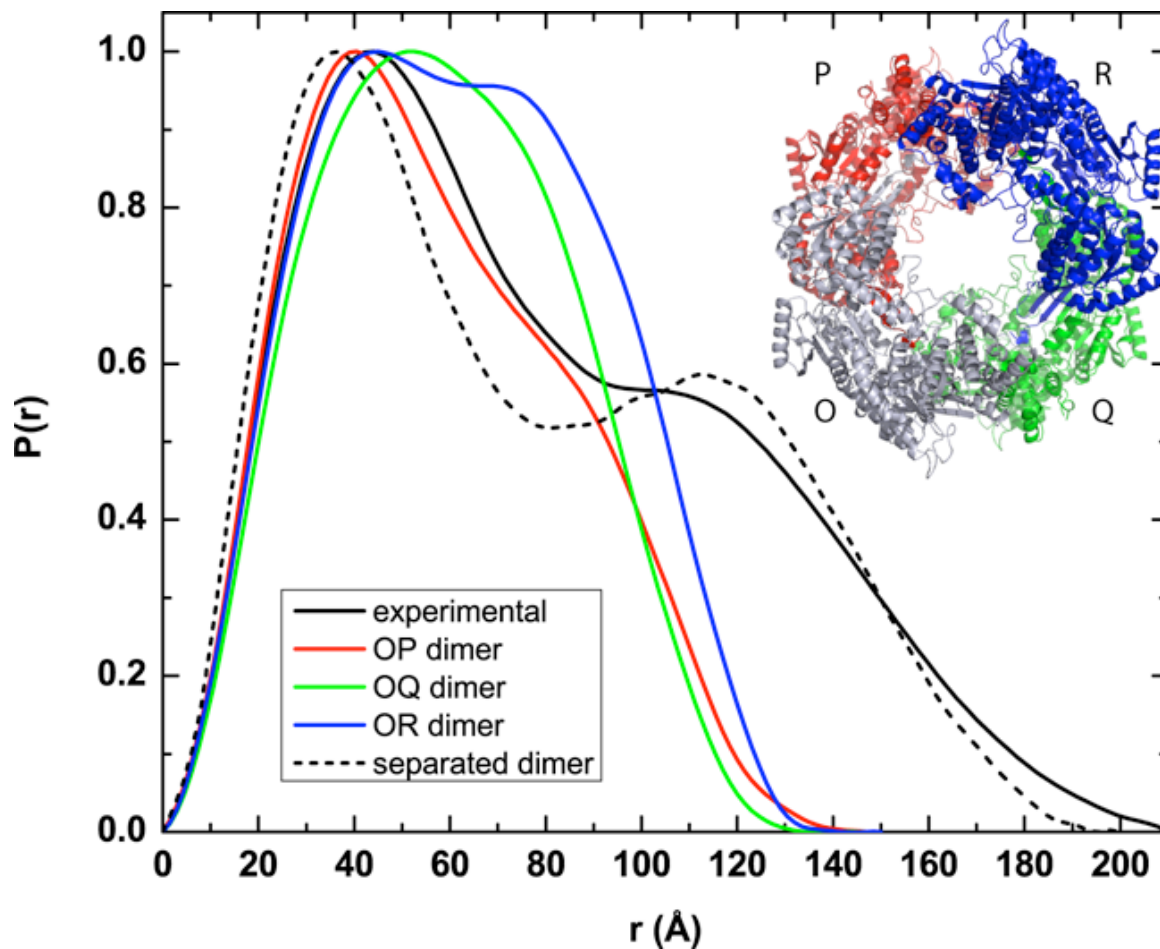


Fig. S5. Comparison of an experimental $P(r)$ curve for EcPutA (solid black) with theoretical curves calculated from the three two-body assemblies of the BjPutA tetramer (red, green, and blue). The chains of the tetramer are labeled O, P, Q, and R, and there are three unique dimeric assemblies: OP, OQ, and OR. The OP dimer corresponds to the one shown in Fig. S1B. The dashed curve was calculated from a model in which two BjPutA protomers were superimposed onto SAXS model 1 (Fig. 7B). The theoretical $P(r)$ curves were calculated using GNOM from theoretical scattering data calculated using FoXS.

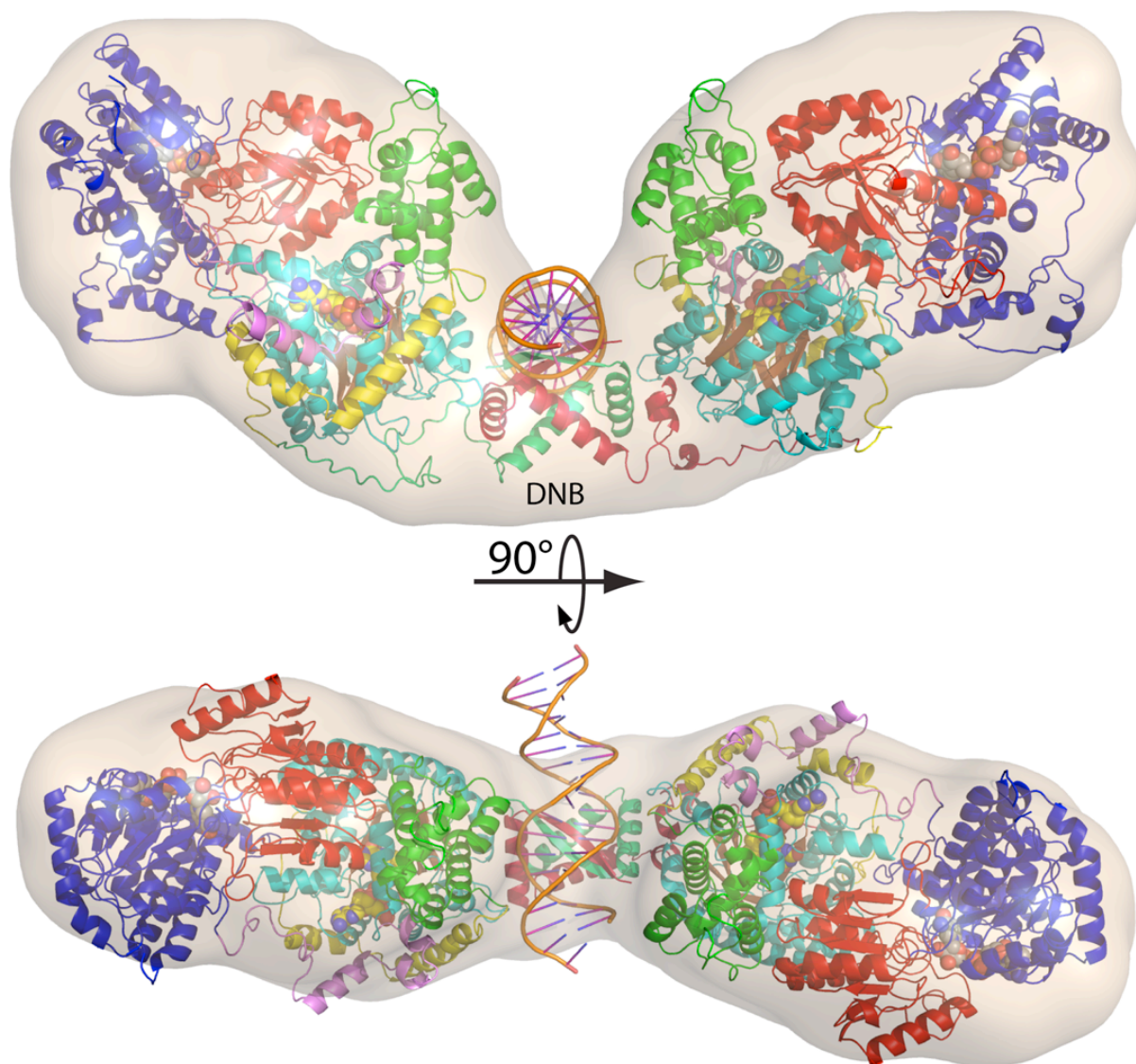


Fig. S6. Model of DNA bound to SAXS model 1. This model was created by superimposing the crystal structure of the EcPutA DNA binding domain complexed with DNA (PDB code 2RBF) onto the DNA-binding domain of SAXS model 1.

Small-angle X-ray Scattering Studies of the Oligomeric State and Quaternary Structure of the Trifunctional Proline Utilization A (PutA) Flavoprotein from *Escherichia coli*

Ranjan K. Singh, John D. Larson, Weidong Zhu, Robert P. Rambo, Greg L. Hura, Donald F. Becker and John J. Tanner

J. Biol. Chem. 2011, 286:43144-43153.

doi: 10.1074/jbc.M111.292474 originally published online October 19, 2011

Access the most updated version of this article at doi: [10.1074/jbc.M111.292474](https://doi.org/10.1074/jbc.M111.292474)

Alerts:

- [When this article is cited](#)
- [When a correction for this article is posted](#)

[Click here](#) to choose from all of JBC's e-mail alerts

Supplemental material:

<http://www.jbc.org/content/suppl/2011/10/19/M111.292474.DC1.html>

This article cites 51 references, 12 of which can be accessed free at <http://www.jbc.org/content/286/50/43144.full.html#ref-list-1>